# Characterisation of the RNA-interference pathway as a Tool for Genetics in the Nascent Phototrophic Endosymbiosis, *Paramecium bursaria*

**Benjamin H. Jenkins[1,2] *†, Finlay Maguire[3] *, Guy Leonard[1,2], Joshua D. Eaton[1], Steven West[1], Benjamin E. Housden[1], David, S. Milner[1,2], & Thomas A. Richards[1,2] †**

[1]Living Systems Institute and Biosciences, University of Exeter, Devon EX4 4QD, UK

[2]Department of Zoology, University of Oxford, 11a Mansfield Road, Oxford OX1 3SZ, UK

[3]Faculty of Computer Science, Dalhousie University, 6050 University Ave, Halifax NS B3H 1W5, Canada

* These authors contributed equally

† Correspondence: ben.jenkins@zoo.ox.ac.uk & thomas.richards@zoo.ox.ac.uk

**KEYWORDS**

symbiosis, interaction, algae, RNAi, Dicer, siRNA

**ABSTRACT**

Endosymbiosis was fundamental for the evolution of eukaryotic complexity. Endosymbiotic interactions can be dissected through forward and reverse-genetic experiments, such as RNA-interference (RNAi). However, distinguishing small (s)RNA pathways in a eukaryote-eukaryote endosymbiotic interaction is challenging. Here, we investigate the repertoire of RNAi pathway protein-encoding genes in the model nascent endosymbiotic system, *Paramecium bursaria–Chlorella* spp. Using comparative genomics and transcriptomics supported by phylogentics, we identify essential proteome components of the small interfering (si)RNA, scan (scn)RNA, and internal eliminated sequence (ies)RNA pathways. Our analyses reveal that copies of these components have been retained throughout successive whole genome duplication (WGD) events in the *Paramecium* clade. We then validate feeding-induced siRNA-based RNAi in *P. bursaria* via knock-down of the splicing factor, *u2af1*, which we show to be crucial to host growth. Finally, using simultaneous knock-down paradox controls to rescue the effect *u2af1* knock-down, we demonstrate that feeding-induced RNAi in *P. bursaria* is dependent upon a core pathway of host-encoded *Dcr1*, *Piwi* and *Pds1* components. Our experiments confirm the presence of a functional, host-derived RNAi pathway in *P. bursaria* that generates 23-nt siRNA, validating use of the *P. bursaria-Chlorella* spp. system to investigate the genetic basis of a nascent endosymbiosis.

33 **INTRODUCTION**

34 Endosymbiosis was fundamental for the evolution of eukaryotic cellular complexity[1–4]. In order to
35 investigate the genetic basis of an emergent endosymbiotic system, we must develop experimentally
36 tractable endosymbiotic model species[5–7]. *Paramecium bursaria* is a ciliate protist which harbours
37 several hundred cells of the green algae, *Chlorella* spp., in a nascent facultative photo-endosymbiosis[8–
38 12]. The algae provide sugar and oxygen derived from photosynthesis, in exchange for amino acids, $CO_2$,
39 divalent cations, and protection from viruses and predators[5,6,13–19]. While the interaction is heritable,
40 the *P. bursaria-Chlorella* spp. system is described as a 'nascent' or 'facultative' endosymbiosis, as both
41 host and endosymbiont can typically survive independently[10,20–23]. *P. bursaria* therefore represents a
42 potentially tractable model system with which to investigate the genetic basis of a nascent
43 endosymbiotic cell-cell interaction.

44 RNA-interference (RNAi) is a form of post-transcriptional gene silencing that is dependent
45 upon conserved small (s)RNA processing pathways[24–26]. The principal components of a functional RNAi
46 pathway are conserved in many eukaryotes[27–29], though loss in some lineages suggests a mosaic
47 pattern of pathway retention[30]. Typically, these pathways rely on size-specific sRNA processing via an
48 endoribonuclease Dicer[26,27], targeted RNA cleavage activity of an Argonaute (AGO-Piwi) containing
49 effector complex[28,31], and RNA-dependent RNA polymerase (RdRP) amplification of either primary or
50 secondary sRNA triggers[32–37]. These triggers may include partially degraded mRNA cleavage
51 products[36], exogenous sRNA[36], or full length mRNA transcripts[32], suggesting that RdRPs may have
52 broader functions in some systems.

53 In ciliates, multiple whole genome duplication (WGD) events have led to the rapid expansion
54 of gene families encoding RNAi components[38–40], resulting in a subsequent diversification of protein
55 function. Example functions include transposon elimination, nuclear rearrangement, and
56 transcriptional regulation[32,35,41–45]. Elegant investigation of the non-photo-endosymbiotic model
57 system, *Paramecium tetraurelia,* has identified three distinct classes of RNAi pathway in *Paramecium*.
58 The ciliate-specific scan (scn)RNA (25-nt) and internal eliminated sequence (ies)RNA (~28-nt)
59 pathways are endogenous, and function primarily to eliminate the bulk of noncoding DNA present in
60 the germline micronuclear genome during development of the somatic macronucleus[35,41–43,46,47].
61 *Paramecium* also encodes a short-interfering (si)RNA (23-nt) pathway capable of processing both
62 exogenously[48–51] and endogenously[32,44] derived RNA precursors. Although siRNA is believed to have
63 evolved to protect against foreign genetic elements (such as viruses, transposons and transgenes)[52],
64 some siRNA-based RNAi factors have also been implicated in the regulation of endogenous
65 transcriptome expression in the non-photo-endosymbiotic model system, *P. tetraurelia*[32].

66 In the photo-endosymbiotic *P. bursaria-Chlorella* spp. system, the existence of a functional
67 siRNA-based RNAi pathway would provide an experimental approach to knock-down gene expression
68 via the delivery of exogenously derived dsRNA homologous to a target transcript[33,48]. Preliminary
69 evidence suggests that siRNA-based RNAi can be induced in *P. bursaria* (110224 strain)[53]; however, a
70 comprehensive analysis with appropriate controls has yet to be conducted. To demonstrate direct
71 evidence of an RNAi-mediated effect, one would need to rescue a putative phenotype through
72 targeted inhibition of the RNAi-knock-down machinery. Such controls are of paramount importance
73 when conducting genetic knock-down experiments in a complex endosymbiotic system, and the
74 presence of a eukaryotic green algal endosymbiont in *P. bursaria* necessitates caution. RNAi has been
75 reported in some green-algal species[54], and thus it is important that controlled experimental
76 characterisation of these distinct pathways be conducted before genetic knock-down in *P. bursaria*
77 can be inferred.

78 Here, we elucidate a cognate repertoire of predicted RNAi component-encoding genes
79 present in *P. bursaria*, confirming that the host genome encodes essential proteome constituents of
80 the siRNA-, scnRNA-, and iesRNA- based RNAi pathways. These include multiple
81 paralogues/orthologues of the pathway components; Dicer, Dicer-like, Piwi (AGO-Piwi), Rdr (RdRP),
82 Cid and Pds1, which have been identified in the non-photo-endosymbiotic model system, *P.*
83 *tetraurelia*[33,34,36]. We trace the occurrence of RNAi protein-encoding genes in the *Paramecium* clade
84 using comparative genomics combined with transcriptomics and supported by phylogenetic analysis,
85 and demonstrate that these genes have been retained throughout successive WGDs. Using an *E. coli*
86 vector feeding-based approach for RNAi induction, we demonstrate functional siRNA-based RNAi in
87 *P. bursaria* via knock-down of a conserved ciliate splicing factor, *u2af1,* which we show to be similar
88 to the *u2af* (65 kDa) constitutive splicing factor present in humans[55,56]. We demonstrate that RNAi-
89 mediated knock-down of *u2af1* results in significant culture growth retardation in *P. bursaria*,
90 suggesting that this gene has a critical function. Finally, we corroborate the function of several siRNA-
91 based RNAi factors in *P. bursaria*; including *Dcr1*, two unduplicated AGO-Piwi factors (*PiwiA1* and
92 *PiwiC1*), and a *Paramecium*-specific *Pds1*, via simultaneous component knock-down to rescue *u2af1*
93 culture growth retardation. Collectively, these data support the presence of a functional, host derived,
94 exogenously-induced siRNA-based RNAi pathway in the *P. bursaria-Chlorella* spp. endosymbiotic
95 system, dependent on *Dcr1*, *Piwi* and *Pds1* protein function.

96 **RESULTS**

97 **Bioinformatic Identification of a Putative RNAi Pathway in *P. bursaria***

98 A feeding-induced siRNA-based RNAi pathway has been validated as a tool for gene knock-down in
99 the non-photo-endosymbiotic ciliate, *P. tetraurelia*[33,34,36,48]. To establish the presence of a comparable
100 pathway in *P. bursaria*, combined genomic- and transcriptomic-analyses were employed to identify
101 putative homologues for all previously characterised *P. tetraurelia* RNAi protein components[33,45]
102 (**Figure 1**). We found that *P. bursaria* encodes a total of five Dicer or Dicer-like endonucleases (*Dcr1*,
103 *Dcr2/3* – **Dataset S1**; *Dcl1/2*, *Dcl3/4* and *Dcl5* – **Dataset S2**), three RdRPs (*Rdr1/4*, *Rdr2* and *Rdr3* –
104 **Dataset S3**), six AGO-Piwi components (*PiwiA1, PiwiA2, PiwiB, PiwiC1, PiwiC2* and *PiwiD*– **Dataset S4**),
105 a single *Paramecium*-specific Pds1 (*Pds1* – **Dataset S5**), and two nucleotidyl transferase (*Cid1/3* and
106 *Cid2* – **Dataset S6**) genes. Among those identified are homologues of the essential feeding-induced
107 siRNA pathway components present in *P. tetraurelia*. In *P. bursaria,* these are; *Dcr1*, *Pds1, Rdr1/4*,
108 *Cid1/3, Cid2,* and putative *PiwiA1* and *PiwiC1* homologues, although we were unable to accurately
109 identify the precise relationship of these *Piwi* paralogues due to lack of phylogenetic resolution
110 (**Dataset S4**). Sequences corresponding to each of these RNAi protein-encoding genes were present
111 in our *P. bursaria* transcriptome dataset, indicating that these host-derived RNAi components are
112 transcriptionally active. These data reveal that *P. bursaria* encodes a putative functional feeding-
113 induced siRNA pathway, indicating that an experimental approach to knock-down gene expression is
114 tractable in this system. Additionally, we show that *P. bursaria* encodes homologues for components
115 of the transgene-induced siRNA pathway, as well as the endogenous ciliate-specific scnRNA and
116 iesRNA pathways involved in nuclear reorganisation and development. For a full list of identified RNAi
117 components, and predicted associated pathways in *P. bursaria*, see **Table 1.**

118 Further analyses were conducted to identify the presence of comparable RNAi pathway
119 components in the algal endosymbiont. For a full overview of the host and endosymbiont
120 transcriptome dataset binning process, please refer to the **Methods**. Using both *P. tetraurelia* and *C.*
121 *reinhardtii* query sequences, our analyses identified a putative homologue for *Dcl1* that clustered with
122 strong support to known green algal Dicer sequences. (**Dataset S7**). No algal homologue for AGO-Piwi
123 or RdRP could be detected in any of the algal-endosymbiont datasets sampled, suggesting that these
124 components are either not transcriptionally active, or are absent altogether in the algal endosymbiont
125 of *P. bursaria*. The absence of RdRP is consistent with its absence in most green algal species
126 sampled[54]. To explore the possible function of a *Dcl* homologue in the sampled endosymbiotic green
127 algae of *P. bursaria*, we conducted sRNA sequencing of algae isolated from the host under standard
128 growth conditions. Our sRNA sequencing data demonstrated that the isolated algal endosymbiont of
129 *P. bursaria* was not actively generating sRNA >20-nt (**Figure S1**), confirming that the mode length of
130 endosymbiont Dicer-derived sRNA does not resemble those of siRNA (23-nt), scnRNA (25-nt) or iesRNA
131 (~28-nt) known to be generated by the non-photo-endosymbiotic model system, *P. tetraurelia*[33–

132 [35,41,42]. This is an important distinction, as it would allow one to ensure that any genetic knock-down
133 approach in the *P. bursaria-Chlorella* spp. system could be attributed to the *Paramecium* host, based
134 on the size of sRNAs generated.

135 **Validation of Feeding-Based RNAi in *P. bursaria***

136 To demonstrate the activity of the putative siRNA-based RNAi pathway in *P. bursaria*, identified in
137 **Figure 1**, we targeted the conserved splicing factor encoding gene, *u2af* [55,56]. Many ciliates genomes
138 are intron-rich and dependent upon splicing for both macronuclear generation and transcription[57],
139 thus it was predicted that knock-down of *u2af* would considerably impact *P. bursaria* growth.
140 Transcriptome analysis revealed that *P. bursaria* encodes three paralogues with sequence similarity
141 to the *u2af* (65 kDa) constitutive splicing factor present in humans[55,56], and indicates that these
142 paralogues likely diverged prior to the radiation of the ciliate clade (**Figure 2a**). Interestingly, the *u2af1*
143 orthologue has been subject to gene duplication prior to diversification of the *Paramecium aurelia*
144 species complex, with >85% copy retention across all species sampled ([n = 39 retained / 11*4
145 predicted], showing 5 putative gene losses in 11 taxa; **Dataset S8**).

146 Phylogenetic analysis indicates that *u2af1* is highly conserved in ciliates, supporting the
147 hypothesis that it may have an essential function (**Figure 2b**). Using an *E. coli* vector-based feeding
148 approach for RNAi induction, delivery of a 500-nt dsRNA fragment corresponding to *u2af1* resulted in
149 significant *P. bursaria* culture growth retardation compared to an empty vector control, consistent
150 with an RNAi effect (**Figure 2c**). Interestingly, retardation to culture growth in response to *u2af1*
151 dsRNA exposure was greater under constant darkness (D 24h), with a mean cell number after 12 days
152 that was significantly less (-84.4%; ***) compared to parallel cultures maintained under standard light-
153 dark (LD 12:12h) conditions. This is consistent with an increased rate of *P. bursaria* feeding in the dark
154 resulting in greater *E. coli* vector uptake[58]. Using mRNA extracted from *P. bursaria* during *u2af1*-RNAi
155 feeding, qPCR revealed a significant reduction in *u2af1* gene expression in response to complementary
156 dsRNA exposure (**Figure 2d**).

157 Next, we designed a 450-nt 'scramble' dsRNA control using a 'DNA shuffle' tool
158 (https://www.bioinformatics.org/sms2/shuffle_dna.html) to randomly shuffle a 450-nt nonsense
159 sequence, ensuring that the resultant 'scramble' dsRNA bore no significant sequence similarity to any
160 *P. bursaria* host or algal endosymbiont transcripts present in the transcriptome datasets. For
161 confirmation of the null effect of 'scramble' dsRNA exposure compared to an empty vector control,
162 see **Figure S2**. Following 'scramble' dsRNA exposure, sRNA isolated from *P. bursaria* was sequenced
163 and mapped against the original 'scramble' DNA template. This allowed us to demonstrate a distinct
164 abundance of sense and antisense 23-nt reads in *P. bursaria* (**Figure 2e**). These results are consistent

165 with previous studies demonstrating *Dicer*-dependent cleavage of dsRNA into 23-nt fragments in *C.*
166 *elegans* and *P. tetraurelia*[26,35]. Collectively, these data confirm the presence of a Dicer-mediated
167 siRNA-based RNAi pathway capable of processing exogenously-derived dsRNA into 23-nt siRNA, and
168 which is induced through the consumption of bacterial cells via phagocytosis.

169 **Investigating *Dcr1* Function**

170 Having demonstrated feeding-based RNAi induction, we investigated putative Dicer function in *P.*
171 *bursaria*. Further dsRNA constructs (Dcr1A, Dcr1B) were designed to specifically target two regions of
172 the *Dcr1* transcript present in *P. bursaria*. A BLASTn search against the *P. bursaria-Chlorella* spp. host
173 and endosymbiont transcript datasets confirmed that the identified dsRNA template from these
174 constructs was predicted to target only *Dcr1,* accounting for all possible 23-nt fragments and allowing
175 for ≤2-nt mismatches. Using mRNA extracted from *P. bursaria* during *Dcr1*-RNAi feeding, qPCR
176 revealed knock-down of *Dcr1* in response to Dcr1A and Dcr1B exposure (**Figure 3a**). Importantly, we
177 found that knock-down was only detected in *Dcr1* when the qPCR amplicon was directly adjacent to
178 the dsRNA target site, with detectable mRNA reduction less evident as the qPCR target amplicon was
179 moved further along the transcript towards the 5' end. This finding suggests that the transcript is only
180 partially degraded upon dsRNA-mediated knock-down – an important consideration for the design of
181 effective RNAi reagents for future experiments.

182 We next checked for the occurrence of any off-target effects arising from Dcr1A/Dcr1B dsRNA
183 exposure, as these may result in knock-down of additional Dicer or Dicer-like components in *P.*
184 *bursaria*. An additional set of qPCR amplicons was designed to target each of the *Dcr2/3*, *Dcl1/2*,
185 *Dcl3/4* and *Dcl5* transcripts identified from our host transcript dataset (**Figure 1**). Full-length
186 sequences were derived from genomic data and compared to respective transcriptome data to ensure
187 that each transcript encompassed the entire open reading frame, allowing us to assess expression
188 from approximately the same relative position on each transcript. A further BLASTn search against the
189 *P. bursaria-Chlorella* spp. host and endosymbiont transcript datasets confirmed that each qPCR
190 amplicon site was specific to the host. Using mRNA extracted from *P. bursaria* during *Dcr1*-RNAi
191 feeding, and qPCR amplicons adjacent to the equivalent position of the Dcr1A/B dsRNA target site,
192 qPCR revealed no significant knock-down in *Dcr2/3*, *Dcl1/2*, *Dcl3/4*, or *Dcl5* transcripts in response to
193 Dcr1A and Dcr1B dsRNA exposure (**Figure 3b**). Indeed, we noted an increase in *Dcr2/3, Dcl1/2* and
194 *Dcl3/4* expression suggesting that these transcripts are potentially being up-regulated to compensate
195 for reduced *Dcr1* expression. These data confirm that exposure to Dcr1A/Dcr1B dsRNA results in
196 specific knock-down of host *Dcr1* in *P. bursaria*.

197 To understand the effect of *Dcr1* knock-down on endogenously triggered *P. bursaria* RNAi
198 function, a size distribution of global host-derived sRNA abundance was compared between cultures
199 exposed to Dcr1A and Dcr1B dsRNA, or a non-hit 'scramble' dsRNA control (**Figure 3c**). A significant
200 reduction in 23-nt sense and antisense sRNA reads was observed upon Dcr1A/Dcr1B dsRNA exposure,
201 accompanied by no significant reduction in any other sRNA read size between 20-30 nt. These data
202 demonstrate that delivery of Dcr1A/Dcr1B dsRNA results in a specific reduction in endogenous 23-nt
203 siRNA abundance, indicative of disruption of predicted *Dcr1* function. An increase in all ≥25-nt sRNA
204 reads upon Dcr1A/Dcr1B dsRNA exposure (**Figure 3c**) may correspond to the increased expression of
205 *Dcr2/3*, *Dcl1/2* and *Dcl3/4* transcripts observed in **Figure 3b** (see also **Table 1**), further corroborating
206 that these additional *Dicer* or *Dicer-like* components are potentially being up-regulated in *P. bursaria*
207 to compensate for disruption of *Dcr1* function. Nonetheless, the absence of significant reduction in all
208 other sRNA sizes (with the exception of 23-nt) indicates that knock-down in response to Dcr1A/Dcr1B
209 dsRNA exposure is effective in specifically reducing host *Dcr1* function in *P. bursaria.*

210 **Validation of *Dcr1*, *Piwi* and *Pds1* Function**

211 Finally, we sought to corroborate the function of a putative feeding-induced siRNA-based RNAi
212 pathway in *P. bursaria*. In an attempt to disrupt *P. bursaria* siRNA-based RNAi function, we exposed
213 cultures to Dcr1A/Dcr1B dsRNA during *u2af1*-RNAi feeding. Simultaneous knock-down of *Dcr1* during
214 *u2af1*-RNAi feeding gave rise to an 'RNAi rescue' phenotype, restoring *P. bursaria* culture growth in
215 *u2af1* dsRNA exposed cultures (**Figure 4a**). Importantly, this effect was significantly greater than the
216 same relative simultaneous delivery of an empty vector control during *u2af1*-RNAi feeding, indicating
217 that rescue of *P. bursaria* culture growth wasn't due to dilution of *u2af1* dsRNA template.

218 We next aimed to corroborate the function of three feeding-induced siRNA-based
219 components that were least supported by phylogenetic inference in *P. bursaria*: *PiwiA1*, *PiwiC1* and
220 *Pds1.* As for *Dcr1*, simultaneous knock-down of either *Pds1*, *PiwiA1*, or *PiwiC1* during *u2af1*-RNAi
221 feeding each gave rise to an 'RNAi recue' phenotype, restoring *P. bursaria* culture growth in *u2af1*
222 dsRNA exposed cultures (**Figure 4b**). *Pds1* is a Paramecium-specific component of feeding-induced
223 siRNA-based RNAi first discovered in *P. tetrauelia*[33]. Sequence homology searches of known functional
224 protein domains could not ascribe a function to Pds1*,* however it was suggested that this protein may
225 play a role in the export of dsRNA from the digestive vacuole into the host cytoplasm[33,36]. Our
226 confirmation that feeding-induced siRNA-based RNAi in *P. bursaria* is dependent upon *Pds1* is
227 important. As the sampled green algae do not encode an identifiable homologue of *Pds1*, this re-
228 iterates that the RNAi effect we have observed is derived from the *P. bursaria* host, and not from the
229 algal endosymbiont.

230 Delivery of *Dcr1*, *PiwiA1*, *PiwiC1* or *Pds1* dsRNA to perturb siRNA-based RNAi function will
231 never provide a complete 'RNAi rescue', since they are themselves important for cellular function.
232 Indeed, partial knock-down of *Dcr1* in this manner may explain why reduction in *Dcr1* transcript
233 expression was not deemed to be statistically significant via qPCR (**Figure 3b**). Mutagenesis screens in
234 *P. tetraurelia* have previously revealed that *Dcr1* null alleles typically result in lethality[33], suggesting
235 that these pathway components have essential functions in *Paramecium*. We propose that partial
236 knock-down of *Dcr1* via an *E. coli* feeding vector-based paradox-approach is therefore preferable to
237 total silencing that would otherwise kill the cell. Perturbation of RNAi through disruption of *Dcr1*
238 (knock-down, rather than knock-out) is sufficient to attenuate the RNAi effect, and thereby provide
239 an appropriate control for inferring a *bona fide* RNAi effect through feeding-induced siRNA-mediated
240 gene knock-down. We have demonstrated that disruption of these essential RNAi components is
241 effective at perturbing both background endogenous (*Dcr1*; **Figure 3c**) and exogenously triggered
242 (*Dcr1, PiwiA1, PiwiC1* and *Pds1*; **Figure 4a/b**) siRNA pathways in *P. bursaria*. Taken together, these
243 data confirm that feeding-induced siRNA-based RNAi in *P. bursaria* is dependent upon host *Dcr1,*
244 *PiwiA1*, *PiwiC1* and *Pds1* function.

245 **DISCUSSION**

246 Here, we have identified the repertoire of cognate RNAi components present in *P. bursaria,* including
247 essential proteome constituents of the siRNA, scnRNA, and iesRNA RNAi pathways. These include
248 orthologues of the pathway components; Dicer, Dicer-like, Piwi, Rdr, Cid and Pds1 that are present in
249 the non-photo-endosymbiotic model system, *P. tetraurelia*. Our comparison across the *Paramecium*
250 clade (**Figure 1**) reveals that many of these components likely originated from the whole genome
251 duplication (WGD) event that occurred prior to the radiation of the *Paramecium aurelia* species
252 complex, which diverged separately from the *P. bursaria* lineage. Importantly, an unusually large
253 number of copies of RNAi-component encoding genes have been retained in the *Paramecium* clade
254 (>80% retention for all components; **Table 2**), exceeding the 40-60% retention rate observed in
255 paralogues of this WGD event across the *Paramecium aurelia* species complex[40]. This observation
256 suggests that these RNAi components are either highly expressed, and thus retention is enforced by
257 gene dosage constraints, and/or have undergone significant neo- or sub-functionalisation driving
258 retention of these paralogues following initial duplication[59]. Our phylogenetic analysis of Dicer, RdRP
259 and AGO-Piwi components (**Datasets S1-4**) supports the occurrence of at least three WGD events
260 within the ciliate group[38–40]. These are hypothesised to have occurred i) after the divergence of the
261 CONThreeP clade (Colpodea, Oligohymenophorea, Nassophorea, Prostomatea, Plagiopylea and
262 Phyllopharyngea)[60,61] from *Oxytricha trifallax* (Spirotrichea) and the broader ciliates, ii) after the
263 divergence of *Paramecium* from *Tetrahymena thermophilia* and remaining Oligohymenophorea, and

264 iii) after the divergence of the *Paramecium aurelia* species complex from the remainder of the
265 *Paramecium* clade (*Paramecium caudatum* and *Paramecium bursaria*).

266 Using an *E. coli* vector feeding-based approach to RNAi induction, we have demonstrated that
267 knock-down of a conserved splicing factor, *u2af1*, results in *P. bursaria* culture growth retardation.
268 Segregation of host germline and somatic nuclei in *Paramecium* makes long term stable [conventional]
269 transformation methods inconsistent and therefore unfeasible for systematic functional genomic
270 profiling. *Paramecium* species are known to conjugate through sexual reproduction approximately
271 every 200 generations[62,63]. This means that a growing library of somatic transformants (featuring RNAi
272 deficient mutations) would need to be maintained and propagated through mitosis to prevent these
273 genetic changes from being lost upon regeneration of the somatic macronucleus. We therefore
274 propose that delivery of exogenously derived dsRNA complementary to a target transcript, in the
275 manner conducted in this study and others[48–51], remains the optimal experimental approach for large-
276 scale gene knock-down surveys in this, and possibly other, ciliate systems.

277 Finally, we have corroborated the function of several RNAi components; including *Dcr1*, two
278 unduplicated Piwi factors (*PiwiA1* & *PiwiC1*), and *Pds1*, via simultaneous component knock-down to
279 rescue *P. bursaria* cell growth, supporting the hypothesis that these factors are required for
280 exogenously-induced siRNA-based RNAi induction in this system. We have demonstrated that, though
281 the algal endosymbiont encodes a putative RNAi pathway including a *Dcl1* homologue, these do not
282 appear to generate sRNAs in the same size range as the host (**Figure S1**). This, together with our
283 assessment of the *Paramecium*-specific factor, *Pds1,* further reinforces that any RNAi effect initiated
284 through a feeding-based approach is likely host-derived. The data presented in this study have allowed
285 us to de-convolute a functional exogenously-inducible siRNA-based RNAi pathway in the
286 endosymbiotic ciliate, *P. bursaria*. We hope that these results will further promote the use of the *P.*
287 *bursaria-Chlorella* spp. endosymbiosis as a key model system to investigate the genetic basis of a
288 nascent endosymbiotic cell-cell interaction.

289 **AUTHOR CONTRIBUTIONS**

290 B.H.J., D.S.M., and T.A.R. conceived and designed the experiments. F.M. conducted transcriptome
291 assembly and binning. B.H.J., D.S.M., and T.A.R. wrote the manuscript. B.H.J., D.S.M., and G.L.
292 conducted experimental work and analysed the data. B.E.H., S.W. and J.D.E aided in conceptual and
293 experimental design, and in conducting experimental work.

294 **ACKNOWLEDGEMENTS**

295 This work was primarily supported by an EMBO YIP award and a Royal Society University Research
296 Fellowship (UF130382) and latterly by an ERC Consolidator Grant (CELL-in-CELL) to T.A.R. S.W. and
297 J.D.E. were supported by awards from the Wellcome Trust (WT107791/Z/15/Z) and the Lister institute.
298 We thank Karen Moore and the University of Exeter Sequence Service for support with the various
299 sequencing projects. We thank Éric Meyer, Institut de Biologie de l'Ecole Normale Supérieure, Paris,
300 for advice during set up of the *P. bursaria* RNAi approach.

301 **DECLARATION OF INTERESTS**

302 The authors declare no competing interests.

303

304 **FIGURES**

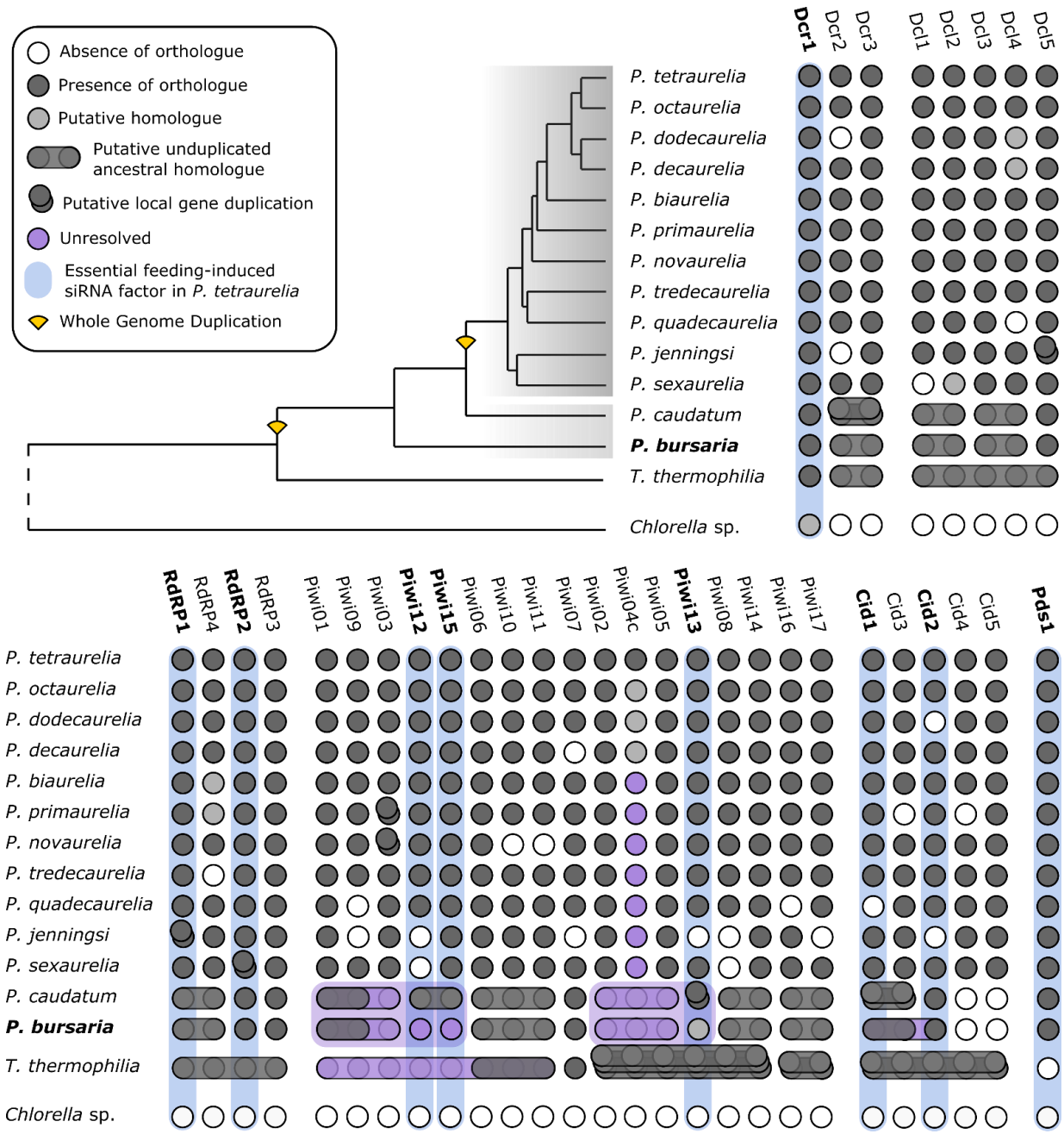


**Figure 1. Identifying a Putative RNAi Pathway in *P. bursaria.*** Coulson plot showing the presence / absence of putative RNAi pathway component-encoding genes, identified from *Paramecium* genome/transcriptome sequence surveys based on shared sequence identity. Genes highlighted in blue represent components essential for feeding-induced siRNA-based RNAi in *P. tetraurelia.* Genes highlighted in purple represent duplicated components with unclear paralogue/orthologue resolution. Stacked genes (single or unduplicated orthologues) represent putative local gene duplications. Phylogeny schematic based on *Dcr1* amino acid alignment (**Dataset S1**), with shaded regions indicating species hypothesised to share the same number of ancestral whole gene duplications (WGDs). For all phylogenies, see **Datasets S1-6**. Nucleotide sequence

315 (https://doi.org/10.6084/m9.figshare.13387811.v1) and amino acid alignment data
316 (https://doi.org/10.6084/m9.figshare.13387631.v1) for putative *P. bursaria* homologues are available
317 at Figshare.

318

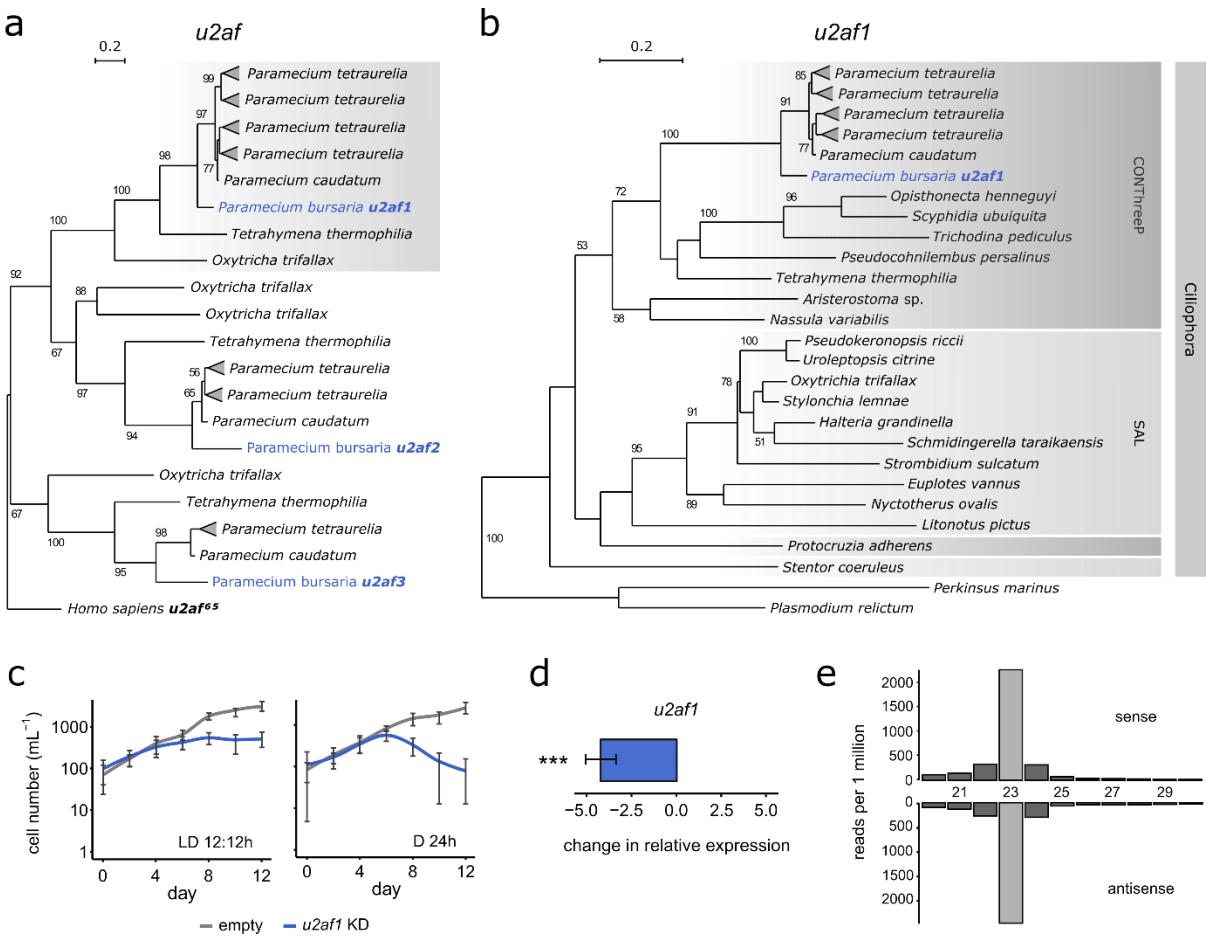


**Figure 2. Validation of Feeding-Based RNAi in *P. bursaria*** (**a**) *U2af* phylogeny (based on 166 sampled aligned amino acid sites) calculated using iqtree with an rtREV+G4 best fit substitution model chosen according to BIC, and with 1,000 non-rapid, non-parametric bootstrap replicates. This phylogeny highlights the three orthologues of *u2af* (65kDa) encoded by *Paramecium*. Note the shaded branch corresponding to the *u2af1* orthologue targeted in this study. (**b**) Specific *u2af1* phylogeny (based on 225 sampled aligned amino acid sites) calculated using iqtree with an LG+G4 best fit substitution model chosen according to BIC, and with 1,000 non-rapid, non-parametric bootstrap replicates. This phylogeny shows the distribution of *u2af1* across the ciliates. Ciliate clades CONThreeP (Colpodea, Oligohymenophorea, Nassophorea, Prostomatea, Plagiopylea and Phyllopharyngea) and SAL (Spirotrichea, Armaphorea and Listomatea) are defined according to Lynn[61,64] and Adl[61,65]. For all phylogenies, bootstrap values above 50 are shown. Amino acid alignment data for putative *P. bursaria* homologues used in the above datasets are available on Figshare (https://doi.org/10.6084/m9.figshare.13387631.v1). (**c**) *P. bursaria* cell number in cultures fed with HT115 *E. coli* expressing *u2af1* dsRNA (blue) or containing an empty vector control (grey). *P. bursaria* cells were resuspended daily into fresh feeding media for 12 days under standard light-dark (LD 12:12h) or constant darkness (D 24h) conditions. Note that the effect of *u2af1* dsRNA exposure was

337 more potent when feeding was conducted under constant darkness, giving rise to a mean cell number
338 after 12 days that was 84.4% less compared to parallel cultures maintained under standard light-dark
339 conditions (***; calculated as $p \leq 0.001$ using a generalized linear model with quasi-Poisson
340 distribution). Data are represented as mean ± SD of five biological replicates. Here and elsewhere, the
341 term 'KD' is used in figure to denote 'knock-down'. (**d**) qPCR of mRNA extracted from day 3 of *u2af1*-
342 RNAi feeding, revealing potent gene knock-down in *P. bursaria* in response to *u2af1* dsRNA exposure.
343 Change in relative expression (ddCT) was calculated for treated (*u2af1* dsRNA) vs untreated (empty
344 vector) control cultures, and normalised against the standardised change in expression of a *GAPDH*
345 housekeeping gene. Data are represented as mean ± SEM of three biological replicates, per treatment.
346 Un-paired dCt values were pooled and averaged prior to calculation of ddCt. Error bars for ddCt values
347 were propagated from the SEM of dCt values. Raw Ct, dCt and error propagation calculations for all
348 ddCt values are available in **Table S3**. Significance for qPCR data calculated as ***$p \leq 0.001$ using a
349 paired t-test. (**e**) Size distribution of sense and antisense sRNAs mapping to a 450-nt 'scramble' dsRNA
350 construct, expressed via transformed *E. coli* fed to *P. bursaria* for three days prior to sRNA extraction
351 and sequencing. Scramble dsRNA presented no significant hit to the identified *P. bursaria* host or
352 endosymbiont transcriptome to ensure that the 23-nt sRNA detected was of definitive exogenous
353 origin.

354

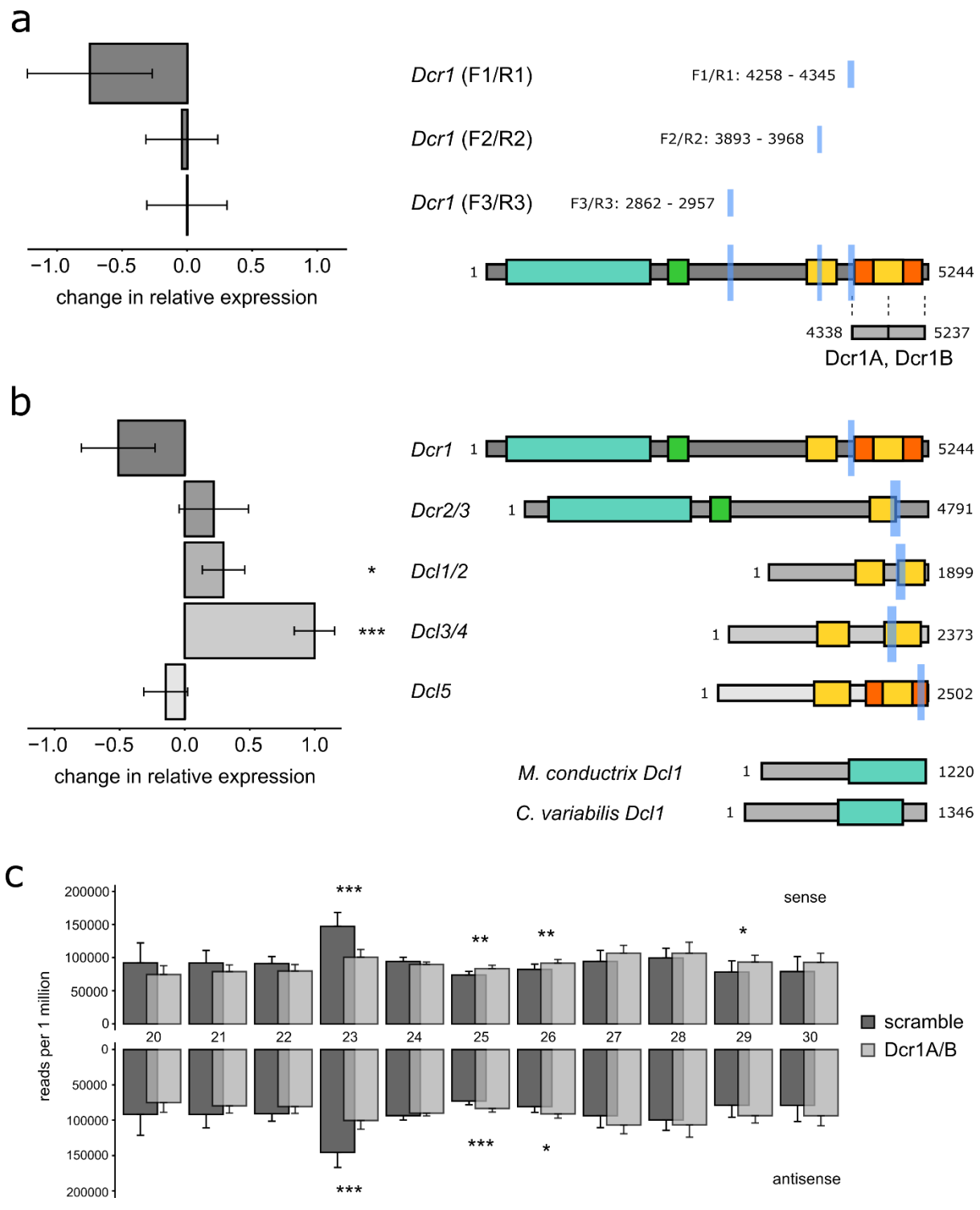


**Figure 3. Investigating *Dcr1* Function** (**a**) qPCR of mRNA extracted from day 3 of *Dicer*-RNAi feeding, revealing *Dcr1* gene knock-down in *P. bursaria* in response to Dcr1A and Dcr1B dsRNA exposure. A schematic representation of *P. bursaria Dcr1* shows the target sites of tandem 500-nt Dcr1A and Dcr1B dsRNA constructs, and amplicon sites of respective *Dcr1* F1/R1, F2/R2 and F3/R3 qPCR primers (light blue). Note the proximity of the amplicon site to the dsRNA target site, relative to the degree of knock-down detected via qPCR. (**b**) Additional qPCR of mRNA extracted from day 3 of *Dicer*-RNAi feeding.

362 Knock-down was not observed in *Dcr2/3*, *Dcl1/2* or *Dcl3/4*, and is inconclusive in *Dcl5*. A schematic
363 representation of all *P. bursaria Dicer* or *Dicer*-like transcripts shows functional domain homology, and
364 amplicon sites of respective qPCR primers (light blue) for each transcript. *M. conductrix Dcl1*
365 demonstrates the divergence of *Dicer* homologues in the *P. bursaria* algal endosymbiont. For all qPCR
366 data, change in relative expression (ddCt) was calculated for treated (Dcr1A+Dcr1B dsRNA) vs
367 untreated (scramble dsRNA) control cultures, and normalised against the standardised change in
368 expression of a *GAPDH* housekeeping gene. Data are represented as mean ± SEM of six un-paired
369 biological replicates, per treatment. Un-paired dCt values were pooled and averaged prior to
370 calculation of ddCt. Error bars for ddCt values were propagated from the SEM of dCt values. Raw Ct,
371 dCt and error propagation calculations for all ddCt values are available in **Tables S4-5**. Significance for
372 qPCR calculated as *$p \leq 0.05$, ***$p \leq 0.001$ using a paired t-test. For all schematic domains: turquoise
373 = Helicase; green = Dicer dimer; yellow = RIBOc; orange = RNC. Amino acid alignment data for putative
374 *P. bursaria* homologues used in the above datasets are available on Figshare
375 (https://doi.org/10.6084/m9.figshare.13387631.v1). For phylogenetic analysis confirming the identity
376 of these *Dicer* and *Dicer*-like components in *P. bursaria*, see **Datasets S1** & **S2.** (**c**) Overlaid size
377 distribution of sense and antisense sRNAs mapping to *P. bursaria* host transcripts during exposure to
378 Dcr1A and Dcr1B dsRNA (light grey), or a non-hit 'scramble' dsRNA control (dark grey). sRNA was
379 sequenced from *P. bursaria* after 7, 8 and 9 days of *E. coli* vector-based RNAi feeding to deliver
380 respective dsRNA. Note the reduction in 23-nt sense and antisense reads upon Dcr1A/Dcr1B dsRNA
381 exposure, accompanied by an increase in ≥25-nt sense and antisense reads. Data are presented as
382 mean ± SD of nine biological replicates (three per time point), and normalised to reads per 1 million
383 20-30 nt reads, per sample. Significance for sRNA abundance calculated as *$p \leq 0.05$, **$p \leq 0.01$, and
384 ***$p \leq 0.001$ by one-way analysis of variance (ANOVA).

385

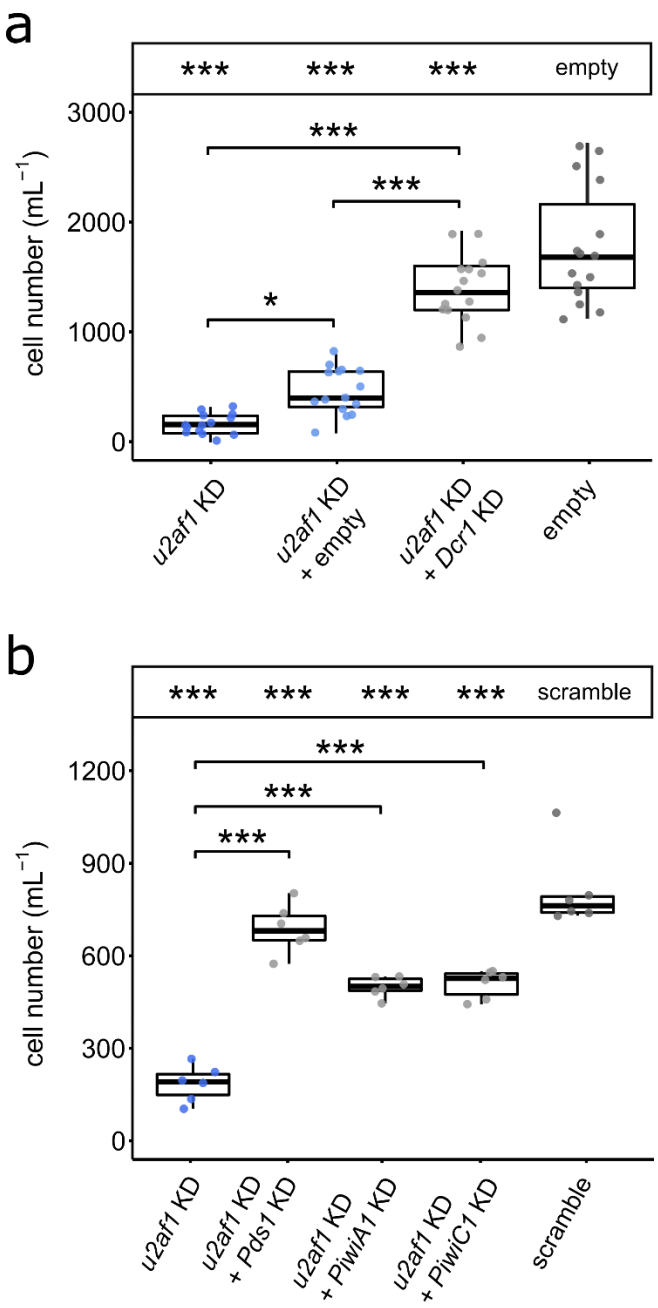


386

387

388 **Figure 4. Validation of *Dcr1*, *Piwi* and *Pds1 Function*** (**a**) *P. bursaria* cell number after 10 days of
389 feeding with HT115 *E. coli* expressing either: *u2af1* dsRNA (dark blue); *u2af1* dsRNA mixed with empty
390 vector (light blue) or *Dcr1* dsRNA (grey); or an empty vector control (white). (**b**) *P. bursaria* cell number
391 after 12 days of feeding with HT115 *E. coli* expressing either: *u2af1* dsRNA (dark blue); *u2af1* dsRNA
392 mixed with *Pds1, PiwiA1,* or *PiwiC1* dsRNA (grey); or a 'scramble' control (dark grey). Multiple vector
393 delivery was conducted at a 50:50 ratio during feeding. Significance calculated as ***$p \leq 0.001$ using
394 a generalized linear model with quasi-Poisson distribution. Boxplot data are represented as max,
395 upper quartile (Q3), mean, lower quartile (Q1) and min values of five biological replicates. Asterisks in
396 the box above each plot correspond to significance compared to empty vector, or 'scramble' dsRNA

397 controls, respectively. Individual data points are shown. Confirmation of the consistent effect of empty
398 vector compared to 'scramble' dsRNA exposure are shown in **Figure S2**.

399 **TABLES**

400 **Table 1. Full list of identified RNAi components and predicted associated pathways in *P. bursaria*.**
401 See also attached file.

| ***P. bursaria* homologue** | **Accession no.[1]** | **Corresponding *P. tetraurelia* homologue[2]** | **Associated pathway in *P. tetraurelia*** | **Reference** |
|---|---|---|---|---|
| *Dcr1* | pending | *Dcr1* | Feeding-induced siRNA (23-nt), Transgene-induced siRNA (23-nt) | 33 |
| *Dcr2/3* | pending | *Dcr2* | - | - |
| | | *Dcr3* | - | - |
| *Dcl1/2* | pending | *Dcl1* | - | 35,41,42 |
| | | *Dcl2* | scnRNA (25-nt) | 35,41,42 |
| *Dcl3/4* | pending | *Dcl3* | scnRNA (25-nt) | 35,41,42 |
| | | *Dcl4* | - | - |
| *Dcl5* | pending | *Dcl5* | iesRNA (~28-nt) | 41,42 |
| *Pds1* | pending | *Pds1* | Feeding-induced siRNA (23-nt) | 33 |
| *Rdr1/4* | pending | *RDR1* | Feeding-induced siRNA (23-nt) | 33 |
| | | *RDR4* | - | - |
| *Rdr2* | pending | *RDR2* | Feeding-induced siRNA (23-nt), Transgene-induced siRNA (23-nt), Endogenous siRNA (23-nt) | 32–34 |
| *Rdr3* | pending | *RDR3* | Transgene-induced siRNA (23-nt), Endogenous siRNA (23-nt) | 32–34 |
| *PiwiA1* | pending | *Ptiwi01* | scnRNA (25-nt) | 66 |
| | | *Ptiwi09* | scnRNA (25-nt) | 66 |
| | | *Ptiwi03* | - | - |
| | | *Ptiwi12* | Feeding-induced siRNA (23-nt) | 33 |
| | | *Ptiwi15* | Feeding-induced siRNA (23-nt) | 33 |
| *PiwiA2* | pending | *Ptiwi06* | - | - |
| | | *Ptiwi10* | - | - |
| | | *Ptiwi11* | - | - |
| *PiwiB* | pending | *Ptiwi07* | - | - |
| *PiwiC1* | pending | *Ptiwi02* | - | - |
| | | *Ptiwi04c* | - | - |
| | | *Ptiwi05* | - | - |
| | | *Ptiwi13* | Feeding-induced siRNA (23-nt), Transgene-induced siRNA (23-nt) | 33 |

| | | | | |
|---|---|---|---|---|
| *PiwiC2* | pending | *Ptiwi08* | - | - |
| | | *Ptiwi14* | Transgene-induced siRNA (23-nt) | [33] |
| *PiwiD* | pending | *Ptiwi16* | - | [33] |
| | | *Ptiwi17* | - | [45] |
| *Cid1/3* | pending | *CID1* | Feeding-induced siRNA (23-nt) | [33] |
| | | *CID3* | Transgene-induced siRNA (23-nt) | [33] |
| *Cid2* | pending | *CID2* | Feeding-induced siRNA (23-nt), Transgene-induced siRNA (23-nt) | [33] |

402

403 [1] Pending NCBI submission, nucleotide (https://doi.org/10.6084/m9.figshare.13387811.v1) and
404 amino acid (https://doi.org/10.6084/m9.figshare.13387631.v1) sequence data for *P. bursaria* RNAi
405 component-encoding genes are available on Figshare

406 [2] For phylogenetic identification of Paramecium homologues, see **Datasets S1-6**

407 **Table 2. Calculation of RNAi component-encoding gene retention rate across the *Paramecium***
408 ***aurelia* species complex.** See also attached file.

| ***P. bursaria* homologue** | **Putative *P. tetraurelia* homologues[1]** | **Predicted copies in *P. aurelia* species complex** | **Actual copies in *P. aurelia* species complex[2]** | **Copy loss in *P. aurelia* species complex** | **Gene retention rate (%)[3]** |
|---|---|---|---|---|---|
| *Dcr1* | 1 | 11 | 11 | 0 | 100.00 |
| *Dcr2/3* | 2 | 22 | 20 | -2 | 90.91 |
| *Dcl1/2* | 2 | 22 | 21 | -1 | 95.45 |
| *Dcl3/4* | 2 | 22 | 21 | -1 | 95.45 |
| *Dcl5* | 1 | 11 | 11 | 0 | 100.00 |
| *Pds1* | 1 | 11 | 11 | 0 | 100.00 |
| *Rdr1/4* | 2 | 22 | 21 | -1 | 95.45 |
| *Rdr2* | 1 | 11 | 11 | 0 | 100.00 |
| *Rdr3* | 1 | 11 | 11 | 0 | 100.00 |
| *PiwiA1* | 5 | 55 | 51 | -4 | 92.73 |
| *PiwiA2* | 3 | 33 | 31 | -2 | 93.94 |
| *PiwiB* | 1 | 11 | 9 | -2 | 81.82 |
| *PiwiC1*[4] | 3 | 33 | 32 | -1 | 96.97 |
| *PiwiC2* | 2 | 22 | 20 | -2 | 90.91 |
| *PiwiD* | 2 | 22 | 20 | -2 | 90.91 |
| *Cid1/3* | 2 | 22 | 20 | -2 | 90.91 |
| *Cid2* | 1 | 11 | 9 | -2 | 81.82 |

409

410 [1] For phylogenetic identification of Paramecium homologues, see **Datasets S1-6**

411 [2] Actual copy number taken from **Figure 1**

412 [3] Not including locally duplicated copies of *Dcl5*, *Rdr1*, *Rdr2* and *Piwi03*

413 [4] *Piwi04c* excluded due to poor phylogenetic resolution

414 **METHODS**

415 ***Culture conditions and media***

416 In all RNAi experiments, *Paramecium bursaria* 186b (CCAP 1660/18) strain was used. For genome
417 analysis, *P. bursaria* 186b strain was used. For transcriptome analysis, *P. bursaria* 186b, CCAP 1660/12
418 and Yad1g1N strains were used.

419 *P. bursaria* cells were cultured in New Cereal Leaf – Prescott Liquid media (NCL). NCL media
420 was prepared by adding 4.3 $mgL^{-1}$ $CaCl_2.2H_2O$, 1.6 $mgL^{-1}$ KCl, 5.1 $mgL^{-1}$ $K_2HPO_4$, 2.8 $mgL^{-1}$ $MgSO_4.7H_2O$
421 to deionised water. 1 $gL^{-1}$ wheat bran was added, and the solution boiled for 5 minutes. Once cooled,
422 media was filtered once through Whatman Grade 1 filter paper and then through Whatman GF/C glass
423 microfiber filter paper. Filtered NCL media was autoclaved at 121°C for 30 mins to sterilise prior to
424 use.

425 NCL medium was bacterized with *Klebsiella pneumoniae* SMC and supplemented with 0.8 $mgL^{-}$
426 $^{1}$ β-sitosterol prior to propagation. *P. bursaria* cells were sub-cultured 1:9 into fresh bacterized NCL
427 media once per month, and maintained at 18°C with a light-dark (LD) cycle of 12:12h.

428 ***Transcriptome analysis***

429 RNA was extracted from *P. bursaria* 186b for transcriptome analysis, using ~$10^6$ host cells from five
430 replicates at three time points over the 12:12 hr LD cycle (6 hr L, 1.5 hr D, and 10.5 hr D). RNA
431 extraction was performed using the RNA PowerSoil Total RNA Isolation Kit (MoBio) following the
432 manufacturers' protocol. Samples were checked for quality using an Agilent TapeStation (High
433 Sensitivity RNA ScreenTape) and a NanoDrop ND-1000, resulting in four low-quality samples which
434 were discarded (RNA Integrity Number <1, NanoDrop concentration <15 $ngµL^{-1}$, or TapeStation <450
435 ng total). RNA for the remaining 11 samples (four 6 hr L, four 1.5 hr D, and three 10.5 hr D) was
436 matched to 400 ng, and library preparation performed using the TruSeq Stranded Total RNA Kit
437 (Illumina) following the manufacturers' protocol. Prepared libraries of 11 samples were then
438 sequenced using a paired-end 120-bp rapid run across two lanes on an Illumina HiSeq 2500, yielding
439 ~1,112 million reads (with a mean of 101 million reads per sample [S.E.M. of 2.9 million reads]). For

440 details of additional transcriptome sequence acquisition from *P. bursaria* CCAP 1660/12, which also
441 included 'single-cell' transcriptome analyses, please refer to the **Supplementary Methods**.

442 Raw reads were trimmed at Q5 in Trimmomatic (v0.32)[67]. Reads were then error corrected using
443 rcorrector (v1.0.0) and digitally normalised using Khmer v1.4.1[68]at a k-mer size of 20 and average
444 coverage of 20. The remaining reads were then assembled using rnaSPAdes (v3.11.1)[69] and Trinity
445 (v2.0.2)[70]. On the basis of RSEM (v1.2.24)[71] and assembly statistics, the Trinity assembly was selected
446 for further analysis.

447 ORFs were called from Trinity assembled transcripts using Transdecoder, using both ciliate
448 (*Tetrahymena*) and universal encodings. The longest peptide sequences were retained for each. The
449 remaining ORFs were then annotated via a BLASTX (v2.2.31) search against a genome database
450 consisting of: *Arabidopsis thaliana*, *Aspergillus nidulans*, *Bacillus cereus* ATCC 14579, *Burkholderia*
451 *pseudomallei* K96243, *Candidatus Korarchaeum cryptofilum* OPF8, *Chlamydomonas reinhardtii*,
452 *Chlorella variabilis* NC64A, *Chlorella vulgaris* C-169, *Escherichia coli* str. K-12 substr. MG1655, *Homo*
453 *sapiens*, *Methanococcus maripaludis* S2, *Oxytricha trifallax*, *Paramecium biaurelia*, *Paramecium*
454 *caudatum*, *Paramecium multimicronucleatum*, *Paramecium primaurelia*, *Paramecium sexaurelia*,
455 *Paramecium tetraurelia*, *Saccharomyces cerevisiae* S288C, *Streptomyces coelicolor* A32, *Sulfolobus*
456 *islandicus* M.14.25, *Tetrahymena borealis*, *Tetrahymena elliotti*, *Tetrahymena malaccensis*,
457 *Tetrahymena thermophila* macronucleus, *Tetrahymena thermophila* micronucleus, and *Ustilago*
458 *maydis*.

459 Assembled transcripts were subsequently binned into either 'host', 'endosymbiont', 'food' or
460 'other' datasets, using a phylogeny-based machine-learning approach
461 (https://github.com/fmaguire/dendrogenous, see **Supplementary Methods**). Binned sequences were
462 further annotated using SignalP (v4.0), TMHMM (v2.0), and BLAST2GO (v4). Each dataset was filtered
463 to remove any sequences with a predicted peptide sequence shorter than 30 amino acids.

464 *P. bursaria* Yad1g1N[22] transcriptome reads were downloaded from DDBJ (Submission
465 DRA000907), and processed using the same approach to assembly and binning as *P. bursaria* 186b
466 dataset described above.

467 ***Phylogenetic analysis***

468 Assembled datasets of ciliate encoded predicted proteins ('host' bin) and universally encoded
469 predicted proteins ('endosymbiont' bin) were searched using BLASTp and a minimum expectation of
470 1e-05, to identify homologues of annotated protein sequences that are putatively encoded by both
471 host and endosymbiont. Proteins predicted from genomic data were downloaded from
472 ParameciumDB[72] for *Paramecium biaurelia, Paramecium caudatum, Paramecium decaurelia,*

473 *Paramecium dodecaurelia, Paramecium jenningsi, Paramecium novaurelia, Paramecium octaurelia,*
474 *Paramecium primaurelia, Paramecium quadecaurelia, Paramecium sexaurelia*, *Paramecium*
475 *tetraurelia* and *Paramecium tredecaurelia*. These were added to a curated dataset of genomic and
476 transcriptomic data from a further 41 ciliate species[73] to assess for homologues throughout the
477 ciliates. Identified homologues were checked against the NCBI non-redundant protein sequences (nr)
478 database via reciprocal BLASTp search.

479 Protein sequences were aligned using MAFFT[74] (v7.471) and masked using TrimAL[75]
480 (v1.4.rev15) allowing for no gaps. Sequences were manually checked in SeaView[76] (v5.0.4), and highly-
481 divergent or identical sequences from the same genomic source were removed. Phylogenies were
482 generated using IQ-TREE (v2.0.3) with 1,000 non-parametric non-rapid bootstraps, using the best fit
483 substitution model calculated with IQ-TREE's inbuilt ModelFinder implementation and according to
484 the Bayesian Inference Criterion (BIC). The models chosen for tree generation are listed in the
485 respective figure legends.

486 ***Gene synthesis and construct design***

487 Sequences for plasmid constructs were synthesised *de novo* by either Genscript or SynBio
488 Technologies, and cloned into an L4440 plasmid vector (Addgene plasmid #1654). Sequences and
489 cloning sites for each plasmid construct are detailed in **Table S1**. All modified constructs were
490 confirmed by Sanger sequencing (Eurofins Genomics).

491 ***RNAi feeding***

492 *P. bursaria* was fed with *E. coli* transformed with an L4440 plasmid construct with paired IPTG-
493 inducible T7 promoters, facilitating targeted gene knock-down through the delivery of complementary
494 double-stranded (ds)RNA. L4440 plasmid constructs were transformed into *E. coli* HT115 competent
495 cells and grown overnight on LB agar (50 $\mu gmL^{-1}$ Ampicillin and 12.5 $\mu gmL^{-1}$ Tetracycline) at 37°C.
496 Positive transformants were picked and grown overnight in LB (50 $\mu gmL^{-1}$ Ampicillin and 12.5 $\mu gmL^{-1}$
497 Tetracycline) at 37°C with shaking (180 rpm). Overnight pre-cultures were back-diluted 1:25 into 50
498 mL of LB (50 $\mu gmL^{-1}$ Ampicillin and 12.5 $\mu gmL^{-1}$ Tetracycline) and incubated for a further 2 hours under
499 the same conditions, until an $OD_{600}$ of between 0.4 and 0.6 was reached. *E. coli* cultures were then
500 supplemented with 0.4 mM IPTG to induce template expression within the L4440 plasmid, and
501 incubated for a further 3 hours under the same conditions. *E. coli* cells were pelleted by centrifugation
502 (3100 x *g* for 2 mins), washed with sterile NCL media, and pelleted once more. *E. coli* cells were then
503 re-suspended in NCL media supplemented with 0.4 mM IPTG, 100 $\mu gmL^{-1}$ Ampicillin, and 0.8 $\mu gmL^{-1}$
504 β-sitosterol, and adjusted to a final $OD_{600}$ of 0.1.

505 *P. bursaria* cells were pelleted by gentle centrifugation in a 96-well plate (10 mins at 800 x *g*),
506 taking care not to disturb the cell pellet by leaving 50 µl of supernatant, and re-suspended 1:4 into
507 200 µl of induced *E. coli* culture media (to make 250 µl total). Feeding was conducted daily for up to
508 14 days using freshly prepared bacterized media.

509 ***qPCR analysis***

510 RNA was extracted from *P. bursaria* 186b for gene expression analysis after three days of RNAi feeding.
511 *P. bursaria* cells (~$10^3$ per culture) were pelleted by gentle centrifugation (800 x *g* for 10 mins), snap-
512 frozen in liquid nitrogen, and stored at -80°C. RNA extraction was performed using TRIzol reagent
513 (Invitrogen), following the manufacturer's protocol after re-suspending each pellet in 900 µl TRIzol
514 reagent. RNA was precipitated using GlycoBlue Co-precipitant (Invitrogen) to aid RNA pellet
515 visualisation, and then cleared of residual DNA using the TURBO DNA-*free* Kit (Ambion), following the
516 manufacturer's protocol for routine DNase treatment.

517 RNA was reverse transcribed into single stranded cDNA using the SuperScript® III First-Strand
518 Synthesis SuperMix (Invitrogen), following the manufacturer's protocol. Quantitative PCR (qPCR) was
519 performed in a StepOnePlus Real-Time PCR system (Thermo Fisher Scientific). Reaction conditions
520 were optimised using a gradient PCR, with a standard curve determined using 10-fold dilutions of *P.*
521 *bursaria* cDNA: *u2af1* (slope: -3.525; $R^2$: 0.994; efficiency: 92.157%), *dcr1* (slope: -3.400; $R^2$: 0.998;
522 efficiency: 96.862%), *dcr2/3* (slope: -3.395; $R^2$: 0.996; efficiency: 97.050%), *dcl1/2* (slope: -3.494; $R^2$:
523 0.999; efficiency: 93.281%), *dcl3/4* (slope: -3.280; $R^2$: 0.999; efficiency: 101.767%), *dcl5* (slope: -3.411;
524 $R^2$: 0.999; efficiency: 96.416%), and *GAPDH* (slope: -3.427; $R^2$: 1.000; efficiency: 95.802%), using
525 StepOne software v2.3. Each 20 µL reaction contained 10 µL PowerUp SYBR Green Master Mix
526 (Thermo Fisher Scientific), 500 mM each primer and 1 µL (50 ng) cDNA. Primers pairs for each reaction
527 are listed in **Table S2**. Each reaction was performed in duplicate for each of 3 biological replicates,
528 alongside a 'no-RT' (i.e. non-reverse transcribed RNA) control to detect any genomic DNA
529 contamination. Cycling conditions were as follows: UDG activation, 2 mins at 50°C and DNA
530 polymerase activation, 2 mins at 95°C, followed by 40 cycles of 15 secs, 95°C and 1 min at 55-65°C
531 (*u2af1* (57°C), *dcr1* (60°C), *dcr2/3* (60°C), *dcl1/2* (60°C), *dcl3/4* (60°C), *dcl5* (60°C), and *GAPDH* (60°C)).
532 Each reaction was followed by melt-curve analysis, with a 60-95°C temperature gradient (0.3°C $s^{-1}$),
533 ensuring the presence of only a single amplicon, and ROX was used as a reference dye for calculation
534 of $C_T$ values. $C_T$ values were then used to calculate the change in gene expression of the target gene
535 in RNAi samples relative to control samples, using a derivation of the $2^{-\Delta\Delta CT}$ algorithm[77].

536 ***sRNA isolation and sequencing***

537 Total RNA for sRNA sequencing was extracted from *P. bursaria* (or free-living algal) cultures using
538 TRIzol reagent (Invitrogen), as detailed above. To isolate sRNA from total RNA, samples were size
539 separated on a denaturing 15% TBE-Urea polyacrylamide gel. Gels were prepared with a 15 mL mix
540 with final concentrations of 15% Acrylamide/Bis (19:1), 8M Urea, TBE (89 mM Tris, 89 mM Borate, 2
541 mM EDTA), and the polymerisation started by the addition of 150 µL 10% APS (Sigma-Aldrich) and 20
542 µL TEMED (Sigma-Aldrich). Gels were pre-equilibrated by running for 15 mins (200 V, 30 mA) in TBE
543 before RNA loading. The ladder mix consisted of 500 ng ssRNA ladder (50-1000nt, NEB#N0364S), and
544 5-10 ng of each 21 & 26-nt RNA oligo loaded per lane. The marker and samples were mixed with 2X
545 RNA loading dye (NEB) and heat denatured at 90 °C for 3 mins before snap cooling on ice for 2 min
546 prior to loading. Blank lanes were left between samples/replicates to prevent cross-contamination
547 during band excision. Gels were then run for 50 mins (200V, 30 mA).

548 Once run, gels were stained by shaking (60 rpm) for 20 mins at RT in a 40 mL TBE solution
549 containing 4 µL SYBR® Gold Nucleic Acid Gel Stain. Bands of the desired size range (~15-30 nt) were
550 visualised under blue light, excised and placed into a 0.5 mL tube pierced at the bottom by a 21-gauge
551 needle, resting within a 1.5 mL tube, and centrifuged (16,000 x *g* for 1 min). 400 µL of RNA elution
552 buffer (1M Sodium acetate pH 5.5 and 1mM EDTA) was added to the 1.5 mL tube containing
553 centrifuged gel slurry, and the empty 0.5 mL tube discarded. Gel slurry was manually homogenized
554 until dissolved using a 1 mL sterile plunger and incubated at RT for 2 hours with shaking at 1,400 rpm.

555 Solutions containing RNA elution buffer and gel slurry were transferred to a Costar Spin-X 0.22
556 µm filter column and centrifuged (16,000 x *g* for 1 min). The filter insert containing acrylamide was
557 discarded. 1 mL of 100% EtOH was added to each solution, alongside 15 µg of GlycoBlue™
558 Coprecipitant (Invitrogen) to aid sRNA pellet visualisation, and stored overnight at -80°C to precipitate.
559 Precipitated solutions were centrifuged at 4°C (12,000 x *g* for 30 mins), and the supernatant discarded.
560 sRNA pellets were washed with 500 µL of cold 70% EtOH (12,000 x *g* for 15 mins at 4°C), and air dried
561 in a sterile PCR hood for 10 mins, before re-suspending in 15 µL of RNAse-free water and storage at -
562 80°C.

563 ***sRNA-seq and read processing***

564 sRNA concentrations were determined using an Agilent 2100 Bioanalyzer, following the Agilent Small
565 RNA kit protocol, and all samples matched to 0.7 $ngmL^{-1}$ prior to sequencing. Library preparation and
566 subsequent RNA-seq was performed for 54 samples using 50-bp paired-end, rapid run across four
567 lanes on an Illumina HiSeq 2500, yielding ~120-150 million paired-end reads per lane (~9-11 million
568 paired-end reads per sample).

569 The raw paired-end reads from the RNA-seq libraries were trimmed using Trim Galore in order
570 to remove barcodes (4-nt from each 3'- and 5'- end) and sRNA adaptors, with additional settings of a
571 phred-score quality threshold of 20 and minimum length of 16-nt. Result were subsequently checked
572 with FastQC.

573 Trimmed reads were mapped against the 'host' or 'endosymbiont' dataset of assembled
574 transcripts using the HISAT2 alignment program with default settings. Post-mapping, the BAM files
575 were processed using SAMTOOLS and a set of custom scripts
576 (https://github.com/guyleonard/paramecium) to produce a table of mapped read accessions and
577 their respective read lengths. Size distributions of sRNA abundance for each sample were plotted using
578 the R programming language packages; tidyverse, grid.extra and ggplot2 in R Studio (v.1.3.1073).

579

580 **DATA AND SOFTWARE AVAILABILITY**

581 The raw reads generated during transcriptome and sRNA sequencing are available on the NCBI
582 Sequence Read Archive (accessions: SAMN14932981, SAMN14932982). All other datasets are
583 available on Figshare (https://doi.org/10.6084/m9.figshare.c.5241983.v1), under the relevant
584 headings. Custom scripts for host and endosymbiont transcript binning
585 (https://github.com/fmaguire/dendrogenous) and sRNA read processing
586 (https://github.com/guyleonard/paramecium) are available on GitHub.

587

588 **REFERENCES**


589 1. Archibald, J. M. Endosymbiosis and eukaryotic cell evolution. *Curr. Biol.* **25**, R911-921 (2015).
590 2. Keeling, P. J. The number, speed, and impact of plastid endosymbioses in eukaryotic evolution.
591 *Annual Review of Plant Biology* **64**, 583–607 (2013).
592 3. Howe, C. J., Barbrook, A. C., Nisbet, R. E. R., Lockhart, P. J. & Larkum, A. W. D. The origin of
593 plastids. *Philos Trans R Soc Lond B Biol Sci* **363**, 2675–2685 (2008).
594 4. Timmis, J. N., Ayliffe, M. A., Huang, C. Y. & Martin, W. Endosymbiotic gene transfer: organelle
595 genomes forge eukaryotic chromosomes. *Nat. Rev. Genet.* **5**, 123–135 (2004).
596 5. Esteban, G. F., Fenchel, T. & Finlay, B. J. Mixotrophy in ciliates. *Protist* **161**, 621–641 (2010).
597 6. Johnson, M. D. Acquired phototrophy in ciliates: a review of cellular interactions and structural
598 adaptations. *J Eukaryot Microbiol* **58**, 185–95 (2011).
599 7. Pröschold, T., Darienko, T., Silva, P. C., Reisser, W. & Krienitz, L. The systematics of Zoochlorella
600 revisited employing an integrative approach. *Environmental Microbiology* **13**, 350–364 (2011).

601 8. Fujishima, M. & Kodama, Y. Endosymbionts in *Paramecium*. *Eur J Protistol* **48**, 124–37 (2012).
602 9. Siegel, R. W. Hereditary endosymbiosis in *Paramecium bursaria*. *Exp Cell Res* **19**, 239–52 (1960).
603 10. Achilles-Day, U. E. & Day, J. G. Isolation of clonal cultures of endosymbiotic green algae from
604 their ciliate hosts. *J Microbiol Methods* **92**, 355–7 (2013).
605 11. Hoshina, R. & Kusuoka, Y. DNA analysis of algal endosymbionts of ciliates reveals the state of
606 algal integration and the surprising specificity of the symbiosis. *Protist* **167**, 174–184 (2016).
607 12. Zagata, P., Greczek-Stachura, M., Tarcz, S. & Rautian, M. The evolutionary relationships between
608 endosymbiotic green algae of *Paramecium bursaria* syngens originating from different
609 geographical locations. *Folia Biol (Krakow)* **64**, 47–54 (2016).
610 13. Brown, J. A. & Nielsen, P. J. Transfer of photosynthetically produced carbohydrate from
611 endosymbiotic *Chlorellae* to *Paramecium bursaria*. *J. Protozool.* **21**, 569–570 (1974).
612 14. Kato, Y. & Imamura, N. Amino acid transport systems of Japanese *Paramecium* symbiont F36-ZK.
613 *Symbiosis* **47**, 99–107 (2009).
614 15. Kato, Y. & Imamura, N. Effect of sugars on amino acid transport by symbiotic *Chlorella*. *Plant*
615 *Physiol Biochem* **46**, 911–7 (2008).
616 16. Kawakami, H. & Kawakami, N. Behavior of a virus in a symbiotic system, *Paramecium bursaria—*
617 *Zoochlorella*. *The Journal of Protozoology* **25**, 217–225 (1978).
618 17. Summerer, M., Sonntag, B., Hörtnagl, P. & Sommaruga, R. Symbiotic ciliates receive protection
619 against UV damage from their algae: a test with *Paramecium bursaria* and *Chlorella*. *Protist* **160**,
620 233–243 (2009).
621 18. Parker, R. C. Symbiosis in *Paramecium bursaria*. *Journal of Experimental Zoology* **46**, 1–12
622 (1926).
623 19. Ziesenisz, E., Reisser, W. & Wiessner, W. Evidence of de novo synthesis of maltose excreted by
624 the endosymbiotic *Chlorella* from *Paramecium bursaria*. *Planta* **153**, 481–485 (1981).
625 20. Kodama, Y. & Fujishima, M. Cycloheximide induces synchronous swelling of perialgal vacuoles
626 enclosing symbiotic *Chlorella vulgaris* and digestion of the algae in the ciliate *Paramecium*
627 *bursaria*. *Protist* **159**, 483–94 (2008).
628 21. Tanaka, M. *et al.* Complete elimination of endosymbiotic algae from *Paramecium bursaria* and
629 its confirmation by diagnostic PCR. *Acta Protozool* **41**, 255–261 (2002).
630 22. Kodama, Y. & Fujishima, M. Symbiotic *Chlorella variabilis* incubated under constant dark
631 conditions for 24 hours loses the ability to avoid digestion by host lysosomal enzymes in
632 digestive vacuoles of host ciliate *Paramecium bursaria*. *FEMS Microbiol. Ecol.* **90**, 946–955
633 (2014).

634 23. Omura, G. *et al.* A bacteria-free monoxenic culture of *Paramecium bursaria*: its growth
635 characteristics and the re-establishment of symbiosis with *Chlorell*a in bacteria-free conditions.
636 *Jpn J Protozool* **37**, (2004).
637 24. Fire, A. *et al.* Potent and specific genetic interference by double-stranded RNA in *Caenorhabditis*
638 *elegans*. *Nature* **391**, 806–11 (1998).
639 25. Timmons, L., Court, D. L. & Fire, A. Ingestion of bacterially expressed dsRNAs can produce
640 specific and potent genetic interference in *Caenorhabditis elegans*. *Gene* **263**, 103–112 (2001).
641 26. Ketting, R. F. *et al.* Dicer functions in RNA interference and in synthesis of small RNA involved in
642 developmental timing in *C. elegans*. *Genes Dev.* **15**, 2654–2659 (2001).
643 27. Carmell, M. A. & Hannon, G. J. RNase III enzymes and the initiation of gene silencing. *Nat. Struct.*
644 *Mol. Biol.* **11**, 214–218 (2004).
645 28. Peters, L. & Meister, G. Argonaute proteins: mediators of RNA silencing. *Mol Cell* **26**, 611–23
646 (2007).
647 29. Cerutti, H. & Casas-Mollano, J. A. On the origin and functions of RNA-mediated silencing: from
648 protists to man. *Curr Genet* **50**, 81–99 (2006).
649 30. Shabalina, S. A. & Koonin, E. V. Origins and evolution of eukaryotic RNA interference. *Trends*
650 *Ecol. Evol. (Amst.)* **23**, 578–587 (2008).
651 31. Ender, C. & Meister, G. Argonaute proteins at a glance. *J Cell Sci* **123**, 1819–23 (2010).
652 32. Karunanithi, S. *et al.* Exogenous RNAi mechanisms contribute to transcriptome adaptation by
653 phased siRNA clusters in *Paramecium*. *Nucleic Acids Res* **47**, 8036–8049 (2019).
654 33. Marker, S., Carradec, Q., Tanty, V., Arnaiz, O. & Meyer, E. A forward genetic screen reveals
655 essential and non-essential RNAi factors in *Paramecium tetraurelia*. *Nucleic Acids Res* **42**, 7268–
656 80 (2014).
657 34. Marker, S., Le Mouël, A., Meyer, E. & Simon, M. Distinct RNA-dependent RNA polymerases are
658 required for RNAi triggered by double-stranded RNA versus truncated transgenes in
659 *Paramecium tetraurelia*. *Nucleic Acids Res* **38**, 4092–107 (2010).
660 35. Lepère, G. *et al.* Silencing-associated and meiosis-specific small RNA pathways in *Paramecium*
661 *tetraurelia*. *Nucleic Acids Res* **37**, 903–915 (2009).
662 36. Carradec, Q. *et al.* Primary and secondary siRNA synthesis triggered by RNAs from food bacteria
663 in the ciliate *Paramecium tetraurelia*. *Nucleic Acids Res* **43**, 1818–33 (2015).
664 37. Aoki, K., Moriguchi, H., Yoshioka, T., Okawa, K. & Tabara, H. In vitro analyses of the production
665 and activity of secondary small interfering RNAs in *C. elegans*. *EMBO J* **26**, 5007–19 (2007).
666 38. Aury, J. M. *et al.* Global trends of whole-genome duplications revealed by the ciliate
667 *Paramecium tetraurelia*. *Nature* **444**, 171–8 (2006).

668 39. McGrath, C. L., Gout, J.-F., Doak, T. G., Yanagi, A. & Lynch, M. Insights into three whole-genome
669 duplications gleaned from the *Paramecium caudatum* genome sequence. *Genetics* **197**, 1417–
670 1428 (2014).
671 40. Gout, J.-F. *et al.* Universal trends of post-duplication evolution revealed by the genomes of 13
672 *Paramecium* species sharing an ancestral whole-genome duplication.
673 http://biorxiv.org/lookup/doi/10.1101/573576 (2019) doi:10.1101/573576.
674 41. Hoehener, C., Hug, I. & Nowacki, M. Dicer-like enzymes with sequence cleavage preferences.
675 *Cell* **173**, 234-247.e7 (2018).
676 42. Sandoval, P. Y., Swart, E. C., Arambasic, M. & Nowacki, M. Functional diversification of Dicer-like
677 proteins and small RNAs required for genome sculpting. *Dev Cell* **28**, 174–88 (2014).
678 43. Malone, C. D., Anderson, A. M., Motl, J. A., Rexer, C. H. & Chalker, D. L. Germ line transcripts are
679 processed by a Dicer-like protein that is essential for developmentally programmed genome
680 rearrangements of *Tetrahymena thermophila*. *Mol Cell Biol* **25**, 9151–9164 (2005).
681 44. Nekrasova, I. V., Владимировна, Н. И., Potekhin, A. A. & Анатольевич, П. А. Diversity of RNA
682 interference pathways in regulation of endogenous and exogenous sequences expression in
683 ciliates *Tetrahymena* and *Paramecium*. *Ecological genetics* **17**, 113–125 (2019).
684 45. Drews, F. *et al.* Two Piwis with Ago-like functions silence somatic genes at the chromatin level.
685 *bioRxiv* 2020.08.24.263970 (2020) doi:10.1101/2020.08.24.263970.
686 46. Chalker, D. L., Fuller, P. & Yao, M.-C. Communication between parental and developing genomes
687 during *Tetrahymena* nuclear differentiation is likely mediated by homologous RNAs. *Genetics*
688 **169**, 149–160 (2005).
689 47. Mochizuki, K. & Gorovsky, M. A. Conjugation-specific small RNAs in *Tetrahymena* have predicted
690 properties of scan (scn) RNAs involved in genome rearrangement. *Genes Dev.* **18**, 2068–2073
691 (2004).
692 48. Galvani, A. & Sperling, L. RNA interference by feeding in *Paramecium*. *Trends Genet* **18**, 11–2
693 (2002).
694 49. Paschka, A. G. *et al.* The use of RNAi to analyze gene function in spirotrichous ciliates. *European*
695 *Journal of Protistology* **39**, 449–454 (2003).
696 50. Slabodnick, M. M. *et al.* The kinase regulator Mob1 acts as a patterning protein for *Stentor*
697 morphogenesis. *PLoS Biol* **12**, (2014).
698 51. Sobierajska, K., Joachimiak, E., Bregier, C., Fabczak, S. & Fabczak, H. Effect of phosducin silencing
699 on the photokinetic motile response of *Blepharisma japonicum*. *Photochem Photobiol Sci* **10**,
700 19–24 (2011).

701 52. Carthew, R. W. & Sontheimer, E. J. Origins and mechanisms of miRNAs and siRNAs. *Cell* **136**,
702 642–655 (2009).
703 53. He, M. *et al.* Genetic basis for the establishment of endosymbiosis in *Paramecium*. *ISME J* **13**,
704 1360–1369 (2019).
705 54. Cerutti, H., Ma, X., Msanne, J. & Repas, T. RNA-mediated silencing in algae: biological roles and
706 tools for analysis of gene function ▿. *Eukaryot Cell* **10**, 1164–1172 (2011).
707 55. Shao, C. *et al.* Mechanisms for U2AF to define 3' splice sites and regulate alternative splicing in
708 the human genome. *Nat Struct Mol Biol* **21**, 997–1005 (2014).
709 56. Cho, S. *et al.* Splicing inhibition of U2AF65 leads to alternative exon skipping. *PNAS* **112**, 9926–
710 9931 (2015).
711 57. Saudemont, B. *et al.* The fitness cost of mis-splicing is the main determinant of alternative
712 splicing patterns. *Genome Biology* **18**, 208 (2017).
713 58. Miura, T., Moriya, H. & Iwai, S. Assessing phagotrophy in the mixotrophic ciliate *Paramecium*
714 *bursaria* using GFP-expressing yeast cells. *FEMS Microbiol Lett* **364**, (2017).
715 59. Ohno, S. Evolution by Gene Duplication. (Springer-Verlag, 1970). doi:10.1007/978-3-642-86659-
716 3.
717 60. Adl, S. M. *et al.* The new higher level classification of eukaryotes with emphasis on the taxonomy
718 of protists. *Journal of Eukaryotic Microbiology* **52**, 399–451 (2005).
719 61. Gao, F. *et al.* The all-data-based evolutionary hypothesis of ciliated protists with a revised
720 classification of the phylum Ciliophora (Eukaryota, Alveolata). *Scientific Reports* **6**, 24874 (2016).
721 62. Beisson, J. *et al.* DNA microinjection into the macronucleus of *Paramecium*. *Cold Spring Harb*
722 *Protoc* **2010**, pdb.prot5364 (2010).
723 63. Jahn, C. L. & Klobutcher, L. A. Genome remodeling in ciliated protozoa. *Annu Rev Microbiol* **56**,
724 489–520 (2002).
725 64. Lynn, D. The ciliated protozoa: characterization, classification, and guide to the literature.
726 (Springer Netherlands, 2008). doi:10.1007/978-1-4020-8239-9.
727 65. Adl, S. M. *et al.* The revised classification of eukaryotes. *J Eukaryot Microbiol* **59**, 429–493
728 (2012).
729 66. Bouhouche, K., Gout, J.-F., Kapusta, A., Bétermier, M. & Meyer, E. Functional specialization of
730 Piwi proteins in *Paramecium tetraurelia* from post-transcriptional gene silencing to genome
731 remodelling. *Nucleic Acids Res.* **39**, 4249–4264 (2011).
732 67. Bolger, A. M., Lohse, M. & Usadel, B. Trimmomatic: a flexible trimmer for Illumina sequence
733 data. *Bioinformatics* **30**, 2114–2120 (2014).

734 68. Crusoe, M. R. *et al.* The khmer software package: enabling efficient nucleotide sequence
735 analysis. *F1000Res* **4**, 900 (2015).
736 69. Bushmanova, E., Antipov, D., Lapidus, A. & Prjibelski, A. D. rnaSPAdes: a de novo transcriptome
737 assembler and its application to RNA-Seq data. *GigaScience* **8**, (2019).
738 70. Haas, B. J. *et al.* De novo transcript sequence reconstruction from RNA-seq using the Trinity
739 platform for reference generation and analysis. *Nat Protoc* **8**, 1494–1512 (2013).
740 71. Li, B. & Dewey, C. N. RSEM: accurate transcript quantification from RNA-Seq data with or
741 without a reference genome. *BMC Bioinformatics* **12**, 323 (2011).
742 72. Arnaiz, O., Meyer, E. & Sperling, L. ParameciumDB 2019: integrating genomic data across the
743 genus for functional and evolutionary biology. *Nucleic Acids Research* gkz948 (2019)
744 doi:10.1093/nar/gkz948.
745 73. Irwin, N. A. T. *et al.* The function and evolution of motile DNA replication systems in ciliates.
746 *Current Biology* (2020) doi:10.1016/j.cub.2020.09.077.
747 74. Katoh, K., Misawa, K., Kuma, K. & Miyata, T. MAFFT: a novel method for rapid multiple sequence
748 alignment based on fast Fourier transform. *Nucleic Acids Res.* **30**, 3059–3066 (2002).
749 75. Capella-Gutiérrez, S., Silla-Martínez, J. M. & Gabaldón, T. trimAl: a tool for automated alignment
750 trimming in large-scale phylogenetic analyses. *Bioinformatics* **25**, 1972–1973 (2009).
751 76. Gouy, M., Guindon, S. & Gascuel, O. SeaView version 4: A multiplatform graphical user interface
752 for sequence alignment and phylogenetic tree building. *Mol. Biol. Evol.* **27**, 221–224 (2010).
753 77. Zhang, J. D., Biczok, R. & Ruschhaupt, M. ddCt: The ddCt algorithm for the analysis of
754 quantitative real-time PCR (qRT-PCR). (Bioconductor version: Release (3.11), 2020).
755 doi:10.18129/B9.bioc.ddCt.
756